https://doi.org/10.5194/egusphere-2025-3069
Preprint. Discussion started: 10 July 2025

Pseudo-Global Warming Simulations Reveal Enhanced Supercell Intensity and Hail Growth in a Future Central European Climate

Lina Lucas[1], Christian Barthlott[1], Corinna Hoose[1], and Peter Knippertz[1]

[1]Institute of Meteorology and Climate Research Troposphere Research (IMKTRO), Karlsruhe Institute of Technology (KIT), Karlsruhe, Germany

Correspondence: Lina Lucas (lina.lucas@kit.edu)

Abstract. Germany is heading toward a future with warmer temperatures due to climate change and potentially cleaner air from electrification and stricter emissions. But how will these evolving environmental conditions affect severe convective storms? This study addresses this question by simulating three supercell events in high resolution using the ICOsahedral Non-hydrostatic model. The events observed during the Swabian MOSES field campaigns in 2021 and 2023 are analysed using the pseudo-global warming approach to assess their evolution in a warmer climate. Aerosol effects were incorporated across all temperature scenarios using a double-moment microphysics scheme, providing detailed insight into the underlying microphysical mechanisms. The results show that higher temperatures generally enhance convection, leading to more intense convective cells, increased precipitation amounts, and more extreme rainfall and hail. Additionally, warmer conditions increase the likelihood of supercell formation and more intense mesocyclones. An important finding is that hailstones grow larger under lower CCN concentrations, and the area affected by large hail expands by up to unit[400]%, indicating growing severity and reach of hail events. In some cases, precipitation increases exceed 7 % K^{-1}, indicating super-Clausius–Clapeyron scaling and suggesting that additional dynamical and microphysical processes amplify rainfall beyond thermodynamic expectations. In addition, lower CCN concentrations are associated with a reduced cold-to-warm rain formation ratio and decreased precipitation efficiency. These aerosol-related effects appear largely independent of temperature, showing consistent patterns across all simulated warming scenarios. These findings indicate the intensity of severe weather events, such as convective storms and flash floods, may increase in a future climate.

1 Introduction

Convective storms, particularly supercells, are significant weather phenomena known for their destructive potential. They can produce severe weather events such as heavy rainfall, strong winds, lightning and large hail (Markowski and Richardson, 2010). During a three-day period around 23 June 2021, multiple severe hailstorms struck southern Germany, France, Switzerland, Austria, and the Czech Republic, culminating in approximately EUR 4 billion of damage (Kunz et al., 2022a). On 23 June 2021, a supercell formed in southwestern Germany, resulting in hailstones reaching maximum diameters of up to 4 cm and ground hail accumulations reaching depths of 30 cm, accompanied by heavy rainfall, and associated flooding.

In recent years, the frequency of weather-related hazards has increased, largely attributed to a warming climate (Hoeppe, 2016;

https://doi.org/10.5194/egusphere-2025-3069
Preprint. Discussion started: 10 July 2025

Rädler et al., 2018; Púčik et al., 2019; Taszarek et al., 2019; Raupach et al., 2021). Especially Germany and the Alps experienced an increase in the annual occurrence of extreme weather events involving lightning, hail exceeding 2 cm in diameter, and wind speeds surpassing 25 $\mathrm{m\,s^{-1}}$ (Rädler et al., 2018).

Recent modelling studies have explored how convective storms respond to rising temperatures using the pseudo-global warming (PGW) approach, which isolates thermodynamic effects by modifying initial and boundary conditions in high-resolution simulations. These studies confirm that warming can intensify deep convection and hail production, though the magnitude and spatial characteristics of these changes vary with model configuration and regional context (Feng et al., 2024; Lin et al., 2024; Tahara et al., 2025). As a result, considerable uncertainty remains regarding how convective hazards such as hailstorms or supercells will evolve in a future climate.

The Clausius–Clapeyron (CC) relationship provides a thermodynamic estimate that atmospheric moisture, and hence precipitation intensity, increases by approximately 6–7 % per degree of warming. However, a number of observational and modelling studies report larger increases, a phenomenon known as super-CC scaling. Such behaviour, where precipitation intensifies beyond 7 % $\mathrm{K^{-1}}$, has been documented in convective and orographic rainfall events (Lenderink and Van Meijgaard, 2008; Haerter and Berg, 2009; Chen et al., 2024). These deviations are thought to result from a combination of dynamic and microphysical processes, including convective organisation (Semie and Bony, 2020), stronger updraughts and latent heating (Lenderink et al., 2017), mesoscale circulations (Fowler et al., 2021), and aerosol–cloud interactions (Martinkova and Kysely, 2020). Large-scale (synoptic) forcing may also play a role. In some cases, stronger synoptic lift or enhanced moisture convergence under warming could intensify convection and contribute to super-CC responses (Fowler et al., 2021). However, the degree to which such effects contribute remains uncertain.

Alongside thermodynamic changes, aerosol concentrations, especially those of cloud condensation nuclei (CCN), play a crucial role in shaping convective storm behaviour (Tao et al., 2007; Barthlott et al., 2022b; Thomas et al., 2023). CCN influence cloud microphysics by affecting droplet formation, growth, and the phase transitions within clouds, which in turn modulate precipitation efficiency, storm dynamics, and hail formation (Fan et al., 2016). Due to stricter emission regulations, anthropogenic aerosol concentrations are projected to decline in North America and Europe (Smith et al., 2011; Leibensperger et al., 2012; Genz et al., 2020), while economic growth in regions such as Asia may lead to increased CCN emissions. In addition to anthropogenic sources, natural aerosols, such as dust, sea salt, volcanic emissions, and biomass burning, also contribute significantly to aerosol variability and may respond to climate drivers like temperature and wind changes (Chin et al., 2014; Van Oldenborgh et al., 2020; Yli-Juuti et al., 2021). Moreover, aerosols remain a major source of uncertainty in climate projections, particularly in simulating extreme weather events (Watson-Parris and Smith, 2022)

Several recent studies have reported that warming alters convective environments, favouring more intense systems while suppressing weaker ones (Rasmussen et al., 2020; Huang et al., 2024; Mallinson et al., 2024; Yang et al., 2024). For instance, Mallinson et al. (2024) observed larger hailstones primarily in the cold season, while Trapp et al. (2019) reported increases throughout the year. Despite growing interest in this area, the future behaviour of extreme convective storms remains uncertain.

In parallel, the forecasting skill of numerical weather prediction (NWP) models has improved considerably over recent decades, thanks to advances in computational power, data assimilation, and parametrisation schemes (Magnusson and Källén, 2013;

Bauer et al., 2015; Buizza, 2019). However, predicting convective precipitation remains a challenge due to the complexity and non-linearity of the involved processes. Storm initiation and evolution are influenced by factors such as synoptic-scale flow, orography, and land surface heterogeneity (Kirshbaum et al., 2018). On a microphysical scale, aerosol–cloud interactions add further uncertainty. Acting as CCN, aerosols influence droplet size and precipitation processes. High CCN concentrations typically result in more numerous, smaller droplets, delaying precipitation onset but potentially intensifying storms through latent heat release at higher altitudes (Seifert et al., 2012). This process is described by the cold-phase convection invigoration theory, which suggests that enhanced freezing of supercooled droplets in polluted environments increases latent heat release in the upper parts of clouds, thereby strengthening updraughts and storm intensity (Rosenfeld et al., 2008). However, previous studies could not confirm this theory using the ICON model (Barthlott et al., 2022a).

Therefore, this study investigates the response of convective storms to global warming and aerosol effects in Germany. Its uniqueness lies in the combined consideration of temperature changes and varying CCN concentrations. This allows for a more comprehensive understanding of how multiple drivers may shape future storm behaviour. The analysis focuses on convective parameters and precipitation characteristics, with particular attention to hail formation and supercell intensities.

To support this integrated analysis, the study employs high-resolution, convection-resolving simulations with the ICOsahedral Non-hydrostatic (ICON) model at a 1 km grid spacing. This fine resolution is essential for explicitly resolving convection, enabling a more accurate representation of storm dynamics and temperature-induced effects. Additionally, the double-moment (2MOM) microphysics scheme of Seifert and Beheng (2006) is used to simulate aerosol effects on both liquid and mixed-phase clouds. By considering both temperature and aerosol influences, this approach provides new insights into the microphysical mechanisms shaping storm intensity, precipitation patterns, and supercell development under changing environmental conditions. The study focuses on real-case simulations of supercell events in Germany, including cases from the Swabian MOSES field campaigns conducted in the summers of 2021 and 2023 in southwestern Germany (Fig. 1).

The remainder of this paper is structured as follows: Section 2 describes the model setup, discusses cases and methodology, Section 3 presents the results of the evaluation, and Section 4 summarises the key findings and conclusions.

2 Method

2.1 Model description

All simulations in this study are conducted using version 2.6.6 of the ICON model (Zängl et al., 2015), which employs a triangular grid structure. The simulation domain covers Germany and parts of neighbouring countries (Fig. 1), with a horizontal grid spacing of 1 km. The vertical coordinates contain 100 terrain-following levels. ICON uses the smooth level vertical (SLEVE) coordinate, allowing a faster transition to a smoother vertical grid (Leuenberger et al., 2010). Furthermore, the model uses the 2MOM microphysics scheme of Seifert and Beheng (2006) to simulate aerosol effects on liquid and mixed-phase clouds. The scheme predicts the mass and number densities of six hydrometeor types: cloud droplets, raindrops, cloud ice, snow, graupel, and hail and parametrises homogeneous and heterogeneous nucleation processes, including cloud condensation

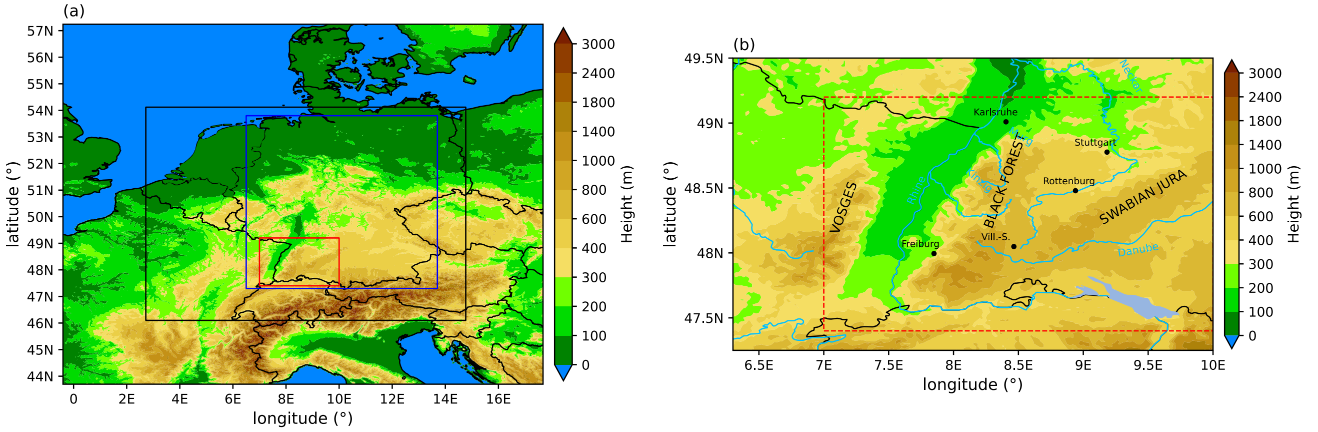

Figure 1. (a) Orography of Central Europe with the black box indicating the simulation domain with a 1 km grid, the blue box denoting the Germany domain. The red box marks the Swabian MOSES field campaign domain. **(b)** Orography of the MOSES area, showing a zoomed-in view of the region marked by the red box in (a). Vill.S. denotes the city of Villingen-Schwenningen, the main measurement site.

Table 1. Model configuration of the ICON simulations.

Model aspect	Setting
Initial and boundary data	7 km ICON-EU analyses, 3 h update
Heterogeneous ice nucleation	Based on typical mineral dust concentrations (Hande et al., 2015)
Homogeneous ice nucleation	Following Kärcher and Lohmann (2002) and Kärcher et al. (2006)
CCN activation	Calculated using pre-calculated activation ratios provided by Segal and Khain (2006)
Deep & shallow convection	Resolved
Land-surface model	Multi-layer land-surface scheme TERRA (Heise et al., 2006)
Turbulence parametrisation	1D based on the prognostic equation for the turbulent kinetic energy (Raschendorfer, 2001)
Radiation scheme	ecRAD (Hogan and Bozzo, 2018), called every 12 min

nuclei activation. Also, turbulence effects on droplet coalescence, raindrop breakup, and size-dependent collision efficiencies are taken into account. Further model settings are given in Table 1.

Label	Concentration	CCN Regime
C1	$100\,\mathrm{cm}^{-3}$	Maritime
C2	$250\,\mathrm{cm}^{-3}$	Intermediate
C3	$1700\,\mathrm{cm}^{-3}$	Continental
C4	$3200\,\mathrm{cm}^{-3}$	Continental Polluted

Table 2. Classification of cloud condensation nuclei (CCN) concentrations and their corresponding labels (Segal and Khain, 2006).

2.2 Simulations overview

To investigate the impact of aerosols on convective storms in a warmer climate, each case is simulated for five different temperatures, with four CCN concentrations applied to each scenario.

1. *Temperature*

   This study investigates the response of convective storms to a warming climate using a PGW approach (Brogli et al., 2023). For each day, five temperature scenarios are simulated, including one reference case. In the remaining four scenarios, the atmospheric temperature is uniformly increased throughout the entire column by increments of $\Delta\mathrm{T} =$+1, +2, +3, +4 K. To maintain consistency with the temperature adjustments, the specific humidity is recalculated using the Clausius-Clapeyron relation under the assumption of constant relative humidity. Additionally, to ensure physical consistency, the pressure at each model level is adjusted by numerically integrating the hydrostatic balance equation:

   $$\frac{dp(z)}{dz} = -g \cdot \frac{p(z)}{R \cdot T(z)} \tag{1}$$

   from the surface to the top of the atmosphere, using the reference simulation's surface pressure as the initial condition (Schär et al., 1996; Kröner et al., 2017). Hereby, g represents the gravitational acceleration, $p(z)$ the pressure at height z, R the specific gas constant for dry air, and $T(z)$ the temperature profile as a function of height. Furthermore, soil temperature, soil surface temperature, and surface temperature are adjusted accordingly to match the imposed temperature increments.

2. *CCN concentration*

   The CCN concentrations used in the simulations are listed in Table 2. C3 is chosen as the reference concentration, as it closely represents present-day CCN levels observed over Germany (Hande et al., 2015). The activation of CCN from aerosol particles is calculated using look-up tables with pre-calculated activation ratios provided by Segal and Khain (2006).

2.3 Analysed cases

This study examines three supercell events from the Swabian MOSES field campaigns conducted in 2021 (Kunz et al., 2022b) and 2023 (Handwerker et al., 2024, submitted). The 2021 campaign aimed to investigate convective storms associated with heavy rain and hail and large-scale heatwaves associated with droughts, while in 2023, the emphasis was on convective storms associated with heavy rain and hail, localised flooding and pollutant inputs to water bodies. It focused on capturing entire events from their onset through development to their impact. Both campaigns were conducted in southwestern Germany, including the Neckar Valley and Swabian Alb (Fig. 1). This area was selected because hailstorms most frequently occur south of Stuttgart and over the Swabian Alb (Kunz and Puskeiler, 2010; Puskeiler et al., 2016). To evaluate the accuracy of the ICON model simulations, results are compared to radar-derived precipitation data from the RADOLAN (Radar Online Adjustment) algorithm provided by the German Weather Service (DWD).

By analysing these simulations across different atmospheric conditions, this study captures a diverse range of convective storm characteristics. Each case represents a distinct convective scenario, highlighting variations in convective cell behaviour (Fig. 2).

2.3.1 Case 1: 23 June 2021

On 23 June 2021, a weakening trough stretched from southern Scandinavia to southern Spain (Fig. 2a). During the day, a shortwave trough moved along its eastern side and reached Germany in the early afternoon. Deep convection occurred with an increase in convective available potential energy (CAPE) in the middle layer over southwest Germany to around $950\,\mathrm{J\,kg^{-1}}$ by midday. Moderately strong winds from a south-westerly direction prevailed in the middle troposphere over Germany. At the surface, a large area of high pressure extended over the North Atlantic, across western Europe, and to northern Germany. A stationary front, a remnant of a multi-core area of low pressure from the previous days, which was now connected to a surface low over Finland, lay over southern Germany and persisted in the following days (Barthlott et al., 2024).

2.3.2 Case 2: 28 June 2021

On 28 June 2021, a trough was located over the west coast of France and covered the area from Great Britain to Spain (Fig. 2c). Over Germany, a slightly strengthening ridge was present, while a short-wave trough passed over southwest Germany in the afternoon. As a result, Germany was affected by moderately strong winds coming from the southwest. A high-pressure field formed over the Atlantic, and pressure values around 580 hPa were reached in the middle troposphere over Central Europe.

2.3.3 Case 3: 22 June 2023

On 22 June 2023, the synoptic setup featured a prominent trough over the North Atlantic and France and a ridge over south-eastern Europe (Fig. 2e). This pattern was associated with a low-pressure system to the northwest and a high-pressure system to the southeast. The resulting pressure gradient led to strong southwesterly flow across Central Europe, advecting warm and moist air and supporting large-scale ascent that contributed to the initiation of convection.

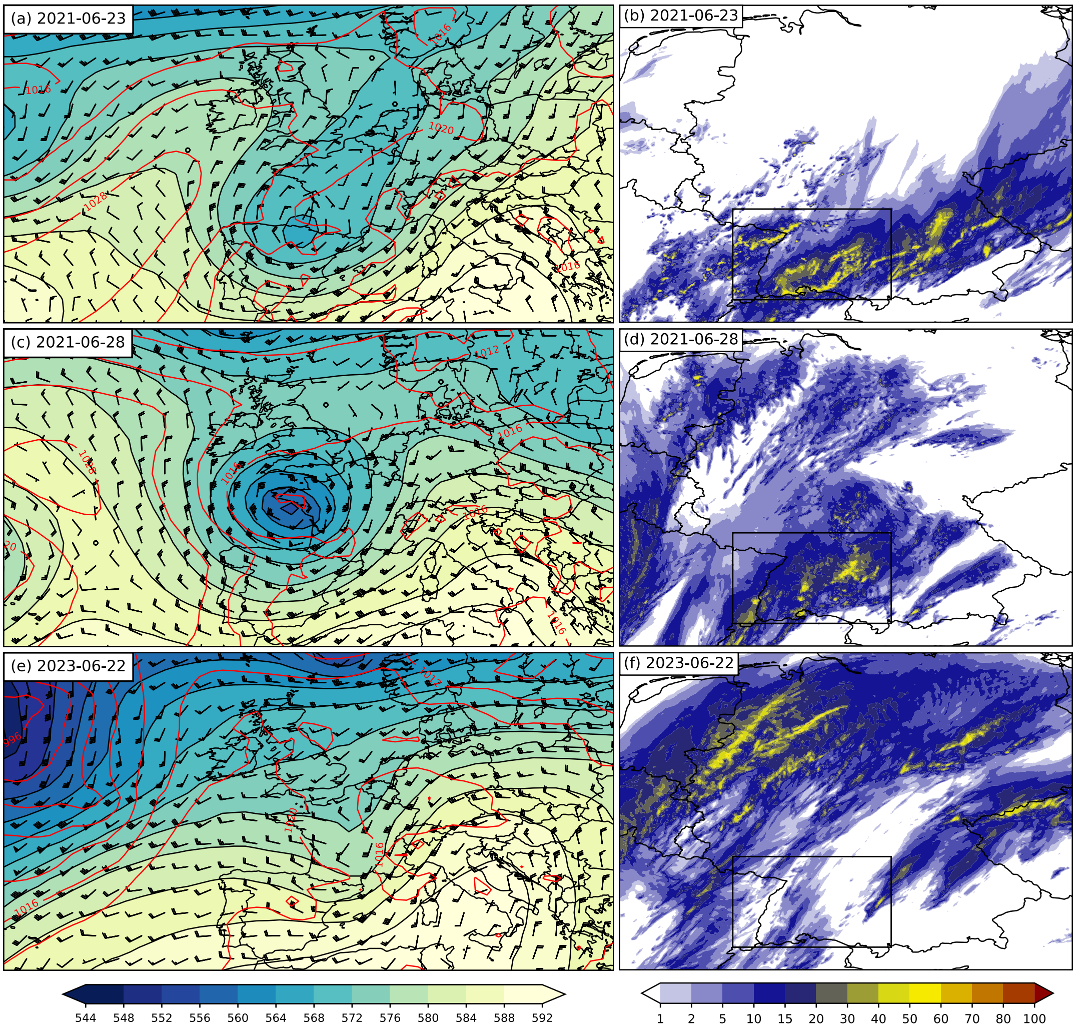

Figure 2. (a, c, e) Global Forecast System (GFS) analysis at 12:00 UTC showing 500 hPa geopotential height (gpdm; shading), sea-level pressure (hPa, red contours), and 500 hPa wind barbs. The colorbar indicates pressure in hPa. **(b, d, f)** Accumulated precipitation over 24 hours across the entire Germany (DE) domain from the reference simulation using continental CCN concentrations (mm). The black box indicates the MOSES domain as in Fig. 1.

3 Results

This chapter presents the results of ICON simulations evaluating the sensitivity of convective storms to atmospheric warming and changes in CCN concentration. The analysis focuses on both thermodynamic and microphysical aspects of storm behaviour. Chapter 3.1 examines the intensity of convective cells, focusing on CAPE, CIN, and updraught helicity as indicators of supercell intensity. It also analyses how changes in temperature and CCN concentrations affect up- and downdraught velocities and cold pool intensities, providing insight into the resulting storm dynamics. Chapter 3.1 investigates precipitation responses, including changes in total and extreme rainfall and hail, deviations from Clausius–Clapeyron scaling, and the evolution of hailstone size distributions under future climate conditions. Chapter 3.3 analyses the frequency and lifetime of convective cells using object-based tracking methods. Finally, Chapter 3.4 explores aerosol–cloud interactions, detailing how CCN concentrations influence hydrometeor content, microphysical process rates, the cold-to-warm rain formation ratio, and precipitation efficiency.

3.1 Intensity of convective cells

In all three cases, CAPE and convective inhibition (CIN) exhibit an increasing trend with rising temperatures (not shown). The rate of increase is relatively uniform across the different simulated temperatures, indicating that the sensitivity of CAPE and CIN to temperature is largely independent of the magnitude of warming, particularly during the time of day when convection is most active. However, the absolute increase in CAPE varies between approximately 80-150 $\mathrm{J\,kg^{-1}}$ across the cases, CIN exhibits only a modest enhancement, typically on the order of a few $\mathrm{J\,kg^{-1}}$. Similar findings have been reported in previous studies (Rasmussen et al., 2020; Huang et al., 2024; Mallinson et al., 2024; Yang et al., 2024), which also observed increased CAPE and CIN in PGW experiments. These results suggest a more favourable environment for stronger convective systems due to enhanced CAPE while simultaneously creating less favourable conditions for weaker trigger mechanisms due to the rise in CIN.

Since the cases involve supercell events, an additional parameter is used to quantify the intensity of such storms. Supercells are characterised by a rotating updraught known as a mesocyclone, which plays a crucial role in their organisation, longevity, and severe weather potential (Markowski and Richardson, 2010). A widely used parameter for identifying such rotating updraughts is the updraught helicity (UH), which quantifies the strength of vertically integrated rotation within a storm. UH can be calculated by integrating the product of the vertical velocity w and the vorticity ζ:

$$\mathrm{UH} = \int w \cdot \zeta \, dz \tag{2}$$

In this study, the product is integrated from 2100 m to 5000 m AGL, focusing on storm rotation in the lower to middle troposphere (Kain et al., 2008). UH provides a useful way to detect and quantify rotating convective storms, as higher values indicate stronger updraught rotation. By plotting UH, the presence and intensity of mesocyclones can be visualised (Weisman and Rotunno, 2000; Thompson et al., 2007). To identify potential supercell regions, a threshold of 75 $\mathrm{m^2\,s^{-2}}$ is applied, following the methodology of Ashley et al. (2023).

To analyse helicity changes across different temperature simulations, the average helicity values exceeding 75 $\mathrm{m^2\,s^{-2}}$ are calculated, along with the number of grid cells meeting this threshold (Fig. 3). The analysis focuses on time frames associated with potential supercell development and the strongest convective activity: between 12:00 and 20:00 UTC for cases 1 and 2 and between 10:00 and 20:00 UTC for case 3. Across all three cases and CCN concentrations, higher temperatures lead to an increase in both the mean helicity values and the number of grid cells exceeding 75 $\mathrm{m^2\,s^{-2}}$. These findings indicate that a warmer future may be associated with an increased likelihood of supercell formation, greater supercell intensity, or a combination of both. However, it is also found that mean helicity values plateau and, in some instances, decrease for the highest simulated temperatures.

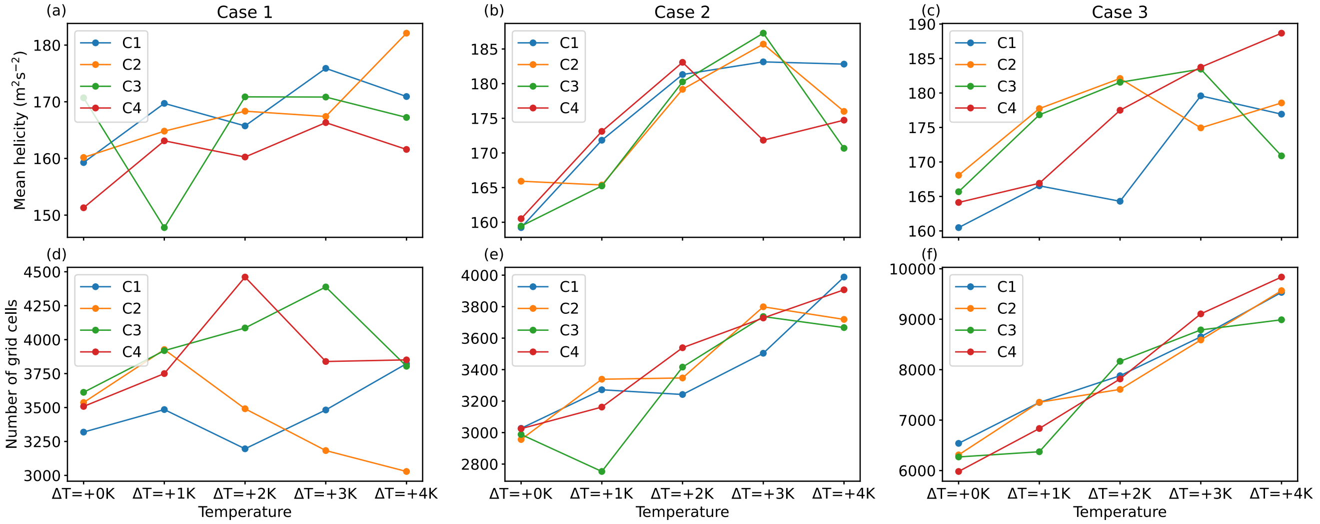

Figure 3. Mean helicity over the whole Germany domain of values larger than 75 $m^2\,s^{-2}$ on **(a)** 23 June 2021 from 12:00 to 20:00 UTC, **(b)** 28 June 2021 from 12:00 to 20:00 UTC, and on **(c)** 22 June 2023 from 10:00 to 20:00 UTC. Number of grid points with helicity values larger than 75 $m^2\,s^{-2}$ **(d)** 23 June 2021 from 12:00 to 20:00 UTC, **(e)** 28 June 2021 from 12:00 to 20:00 UTC, and on **(f)** 22 June 2023 from 10:00 to 20:00 UTC.

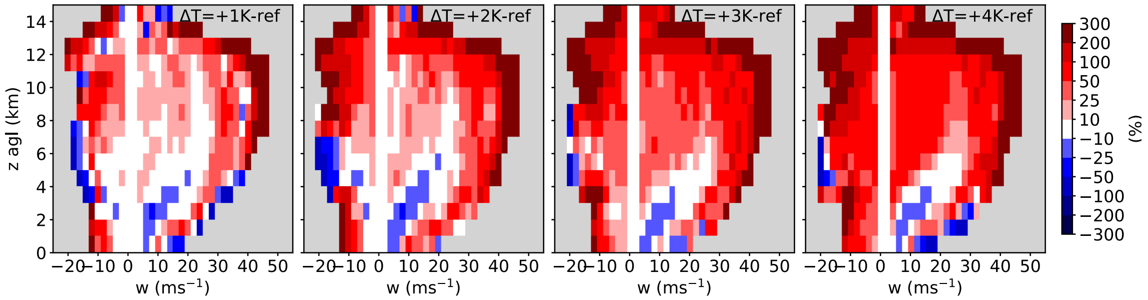

Figure 4. The change in the daily mean updraught and downdraught velocity for different atmospheric temperatures and a continental CCN concentration (C3), shown for the MOSES domain (28 June 2021). The domain is defined in Fig. 1.

While CCN concentrations do not show a uniform impact on helicity values across all simulations, distinct variations are observed in some cases between different CCN scenarios. In contrast, temperature shows a consistent and stronger influence, with helicity values increasing systematically under warmer conditions. Overall, the impact of temperature on helicity is more pronounced than that of CCN concentration.

https://doi.org/10.5194/egusphere-2025-3069
Preprint. Discussion started: 10 July 2025

The influence of atmospheric warming on convective cell dynamics is illustrated in Fig. 4 for the 28 June 2021 case. As temperatures rise, both updraught and downdraught velocities intensify in the upper troposphere, indicating enhanced convective activity under warmer conditions. Updraughts in the range of 0–40 $\mathrm{m\,s^{-1}}$ increase by approximately 50–100 %, while the most intense updraughts show increases exceeding 300 % in the +4 K simulation. A similar pattern is observed for downdraughts: lower intensities increase by 50–100 %, with the strongest downdraughts (10–20 $\mathrm{m\,s^{-1}}$) increasing by more than 300 % under the same warming scenario. This general intensification of vertical motion in the upper troposphere is consistently observed across all three analysed cases. However, it is primarily the moderate up- and downdraughts that show this robust increase in all cases, while the most extreme velocities exhibit more case-to-case variability.

In contrast, changes in CCN concentration influence the frequency and distribution of vertical velocities. For higher CCN concentrations, the occurrence of strong updraughts (20–30 $\mathrm{m\,s^{-1}}$) in the upper troposphere decreases (not shown). While downdraught intensity also weakens in the upper troposphere, a slight increase is observed in the middle to upper troposphere. Near the surface, downdraught strength again diminishes. This vertical structure could be linked to enhanced precipitation loading aloft in a low CCN environment, which contributes to stronger downdraughts at mid-levels but less pronounced impacts near the surface. To further investigate this behaviour, cold pools are analysed.

Cold pools offer additional insight into convective intensity. They consist of volumes of negatively buoyant air that originate from evaporative cooling in precipitating downdraughts (Hirt et al., 2020). They are characterised by negative temperature anomalies, which can be derived using the density potential temperature defined by Hirt et al. (2020) as:

$$\theta_\rho = \theta(1 + 0.608 r_v - r_w - r_i - r_r - r_s - r_g - r_h) \tag{3}$$

where θ is the potential temperature, r_v is the water vapour mixing ratio, and r_w, r_i, r_r, r_s, r_g, and r_g are the mixing ratios of cloud water, cloud ice, rain, snow, graupel, and hail, respectively. The local perturbation of density potential temperature $\theta'_{\rho,0}$ is calculated relative to a spatiotemporal moving average $\bar{\theta}^m_\rho$, using a horizontal window of 166 grid points and a temporal window of 8 hours. To isolate cold pool structures, the domain-mean perturbation is subtracted: $\theta'_\rho = \theta'_{\rho,0} - \bar{\theta}'_{\rho,0}$. Cold pools are identified by applying thresholds: only perturbations below –2 K, associated with precipitation rates exceeding 10 $\mathrm{mm\,hr^{-1}}$, and with horizontal extents greater than 6 km are considered. The remaining cold pool perturbations are used to compute a density distribution function for each temperature and CCN concentration scenario.

Varying CCN concentrations have a systematic influence, as illustrated in Fig. 5. The highest CCN case (C4) exhibits a pronounced peak around –5 K with a narrow distribution and a short tail, indicating frequent but moderate cold pool anomalies. As CCN concentrations decrease, the distributions broaden and develop longer tails, indicating greater variability and a higher occurrence of stronger cold anomalies. This enhanced cold pool intensity at lower CCN concentrations is also reflected in the downdraughts: increased downdraught strength is observed in the lower troposphere under low CCN conditions (not shown). This behaviour is consistent with the known mechanism in which enhanced subcloud evaporative cooling leads to stronger cold pool formation and, consequently, more intense downdraughts. The increased evaporation under low CCN conditions is further promoted by the formation of larger raindrops, which evaporate more efficiently as they fall through the subcloud layer, enhancing cooling.

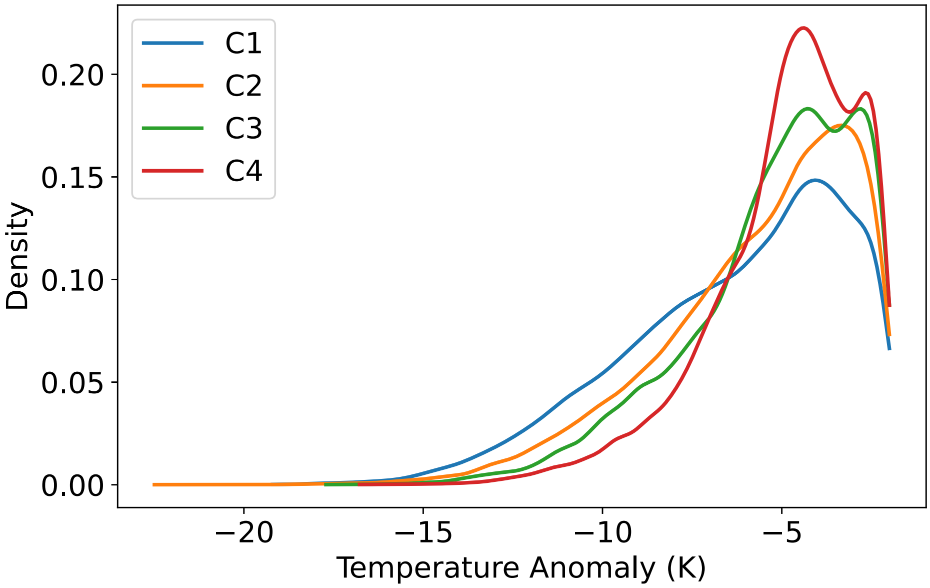

Figure 5. Density distributions of cold pool temperature anomalies for different CCN concentrations, calculated between 06:00 UTC and 24:00 UTC within the MOSES domain on 28 June 2021. The domain is defined in Fig. 1.

3.2 Precipitation

To evaluate changes in precipitation, the behaviour of rain and hail is analysed separately for all days (Fig. 6). First, the total amount of rain and hail is examined. Rain exhibits an increasing trend across all days, with increases ranging from approximately 15 % to 70 % in the +4 K simulation. Hail also increases with rising temperatures, exhibiting a greater relative change compared to rain. On 23 June 2021 and 28 June 2021, hail increases by around 30 %. However, on 22 June 2023, hail increases by nearly 200 %, suggesting that synoptic-scale forcing likely played a role. Synoptic-scale environments significantly influence the response of hailstorms to climate warming, with frontal systems exhibiting a more substantial increase in large hail occurrences compared to other synoptic setups (Fan et al., 2022)

To assess changes in extreme precipitation events, the 95th percentile of rain and hail amounts is analysed. For rain, the 95th percentile consistently increases with temperature, indicating that even heavier rainfall events will occur, heightening the risk of flash floods. On 28 June 2021 and 22 June 2023, extreme rainfall amounts increase by approximately 50 % in a +4 K warming scenario. A similar trend is observed for hail, with a substantial increase in the 95th percentile. On 22 June 2023, extreme hail amounts rise by over 200 %, indicating a strongly increased potential for severe hailstorms and elevated damage risks in a warmer climate.

Next, the number of grid cells experiencing extreme rainfall and hailfall (95th percentile) is evaluated. Again, a notable increase is observed. On 22 June 2023, a +4 K temperature increase results in a 400 % expansion of the area impacted by large hail amounts. This corresponds to an increase from 369 km^2 to 3,995 km^2, representing a dramatic growth from an area com-

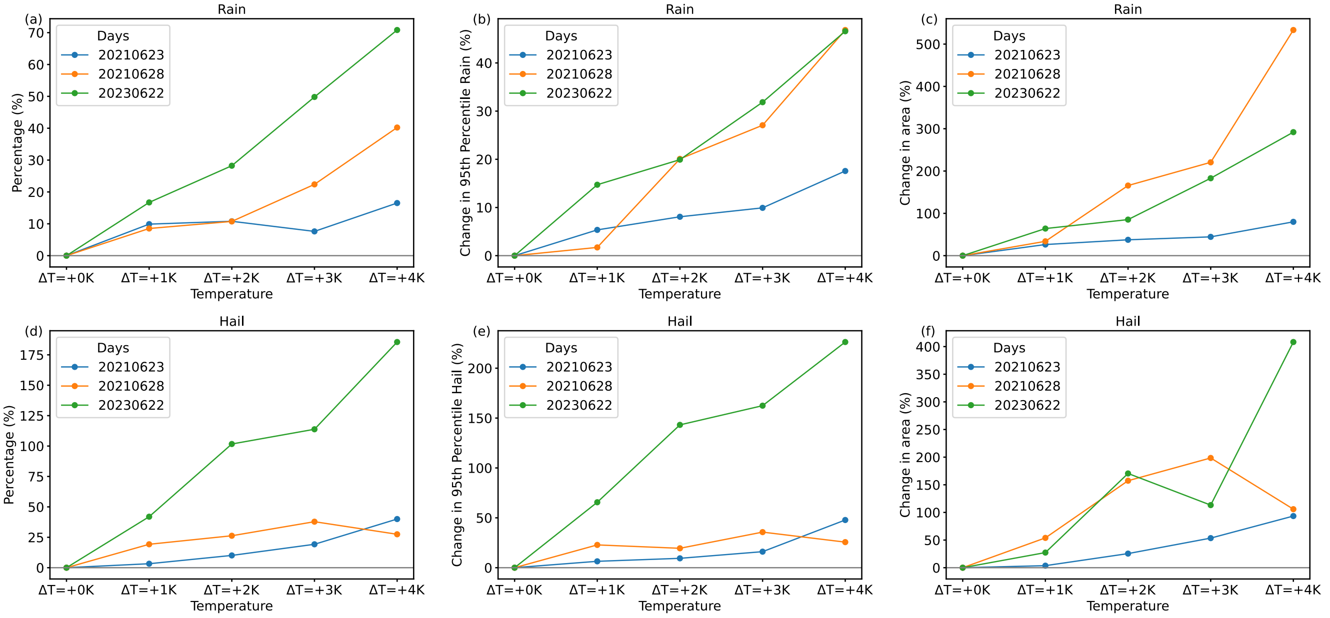

Figure 6. Percentage change of the amount of **(a)** rain and **(d)** hail, the change in the 95th percentile of **(b)** rain and **(e)** hail, and the change in the area affected by **(c)** rain > 45 mm and **(f)** hail > 10 mm (the 95th percentile) for changing atmospheric temperatures on all three simulated days (different line colours) for a continental CCN concentration (C3) and in the MOSES domain. The domain is defined in Fig. 1.

parable to the size of Munich to one comparable to the island of Mallorca. Even the smallest increase, observed on 23 June 2021, amounts to 100 %, representing a doubling of the impacted region.
The effects of CCN concentrations on precipitation will be discussed later in Chapter 3.4.

3.2.1 Hail sizes

Since hail appears to undergo the most significant changes, and because damage assessments are primarily based on hailstone sizes (Kim et al., 2023; Schmid et al., 2024), the influences of higher temperatures and changes in CCN concentrations on hailstone sizes are investigated. The hailstone size distributions are calculated using a generalised Gamma distribution:

$$f(x) = Ax^{\nu}\exp(-\lambda x^{\mu}), \tag{4}$$

whereby ν represents the shape parameter, μ the dispersion parameter and x is the particle mass. A and λ are calculated from the predicted mass and number densities. Different combinations of ν and μ with values between 0 and 1 lead to different distributions. If $\mu = 1$, the function reduces to a classical Γ-distribution, for $\nu = \mu = 1$ the result is the Weibull distribution and for $\nu = \mu = 0$ an exponential distribution is calculated (Seifert and Beheng, 2006). For this evaluation, $\nu = 1$ and $\mu = \frac{1}{3}$ are used, which are the parameters for hail in this model. This function is rewritten as a function of diameter D, using $x = \frac{\pi}{6}\rho D^3$

https://doi.org/10.5194/egusphere-2025-3069
Preprint. Discussion started: 10 July 2025

which is true for spherical particles (Khain et al., 2015):

$$f(D) = N_0' D^{\nu'} \exp(-\lambda' D^{\mu'}), \tag{5}$$

with $N_0' = 3N_0(\frac{\pi}{6}\rho)^{\nu+1}$, $\nu' = 3\nu + 2$, $\lambda' = \lambda(\frac{\pi}{6}\rho)^{\mu}$, and $\mu' = 3\mu$. N_0 represents the intercept parameter and ρ the bulk hydrometeor density.

The resulting mean hail size distributions on the surface for 23 June 2021 are presented in Fig. 7. To assess how hail sizes respond to changes in temperature and CCN concentration, the maxima of the distributions are analysed as indicators of the dominant hailstone size (Fig. 8). The results reveal a systematic increase in hailstone size with increasing temperatures across all CCN concentrations. This occurs despite an elevation of the freezing level by approximately 200 m per degree Celsius, which would typically enhance hail melting and reduce final hail size. Furthermore, lower CCN concentrations are also associated with larger hail sizes. Temperature and CCN concentration exert similarly strong influences on hail size. Given that both future warming and decreasing CCN concentrations are expected, these factors are likely to contribute to the formation of larger hailstones under future atmospheric conditions.

To evaluate the impact of temperature and CCN concentration on the largest hail sizes, the hail size distribution is extended beyond the model's initial output up to the point where the distribution curve returns to a relative frequency of 0.0025. In the model, the particle mass x is constrained by a maximum value x_{max}, which limits the simulated hail size distribution (Fig. 7) and excludes larger hailstones. However, when comparing the extended size distribution curve for larger x with the curve of the model's output, both follow the same trend, indicating that the distribution can be reliably extended to account for larger hailstones. Therefore, the hail sizes corresponding to a distribution value of 0.0025 are determined from the extended hail size distribution curve and analysed using the same approach as for the dominant hailstone sizes. The results reveal an almost identical pattern for the changes in dominant and maximum hailstone sizes (not shown), confirming that not only do medium-sized hailstones grow larger in a warmer climate, but the large hailstones also experience significant growth. These findings are particularly concerning given the high damage potential associated with large hailstones.

3.2.2 Clausius-Clapeyron scaling

To explain the observed increase in precipitation, Clausius–Clapeyron (CC) scaling provides an essential theoretical framework. Although uncertainties persist, it is widely accepted that rising temperatures intensify heavy precipitation events by increasing the atmosphere's water vapour-holding capacity (Hardwick Jones et al., 2010). According to the CC relationship, water vapour content, and consequently precipitation, increases by approximately 6–7 $\%\,\text{K}^{-1}$ (Risser and Wehner, 2017). This study investigates to what extent precipitation changes in convective storm events follow the expected CC scaling, and whether deviations from this rate, known as super-CC responses, can be identified under warming conditions.

In our simulations, water vapour content is adjusted according to CC scaling, ensuring an initial increase close to the predicted 7 $\%\,\text{K}^{-1}$ (not shown). However, accumulated precipitation does not consistently follow this trend, as shown in Fig. 9. In particular, Case 1 and Case 3 exhibit significantly greater increases in precipitation, far exceeding 7 $\%\,\text{K}^{-1}$. On 22 June 2023, precipitation increases by more than 17 $\%\,\text{K}^{-1}$, while on 23 June 2021, an increase of over 9 $\%\,\text{K}^{-1}$ was observed. These

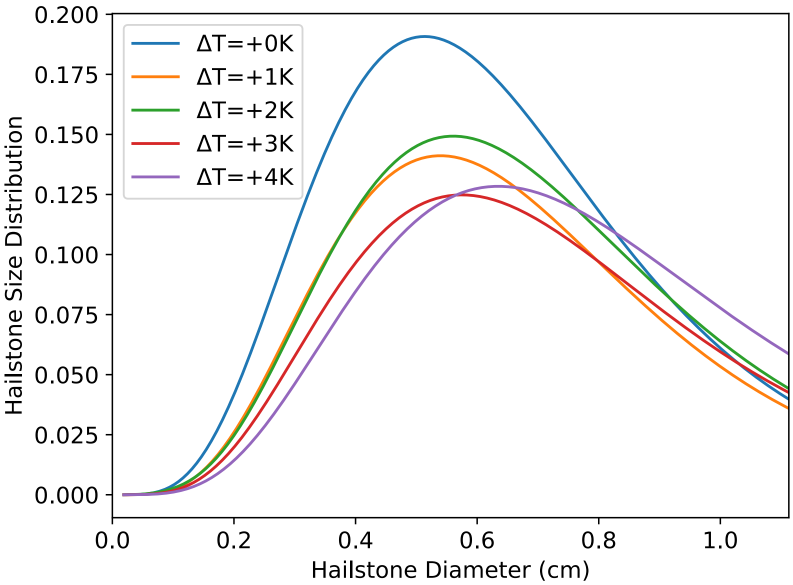

Figure 7. Mean hailstone size distribution in the MOSES domain for all simulation temperatures using the continental CCN concentration (C3) on 23 June 2021. The domain is defined in Fig. 1. Line colours indicate the different temperature scenarios.

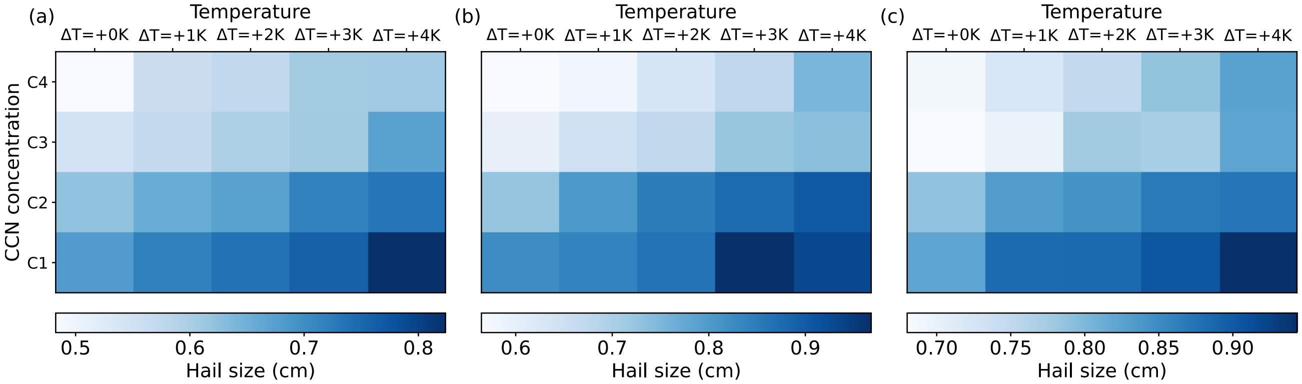

Figure 8. Dominant hailstone sizes for different temperature regimes and CCN concentrations on **(a)** 23 June 2021, **(b)** 28 June 2021, and **(c)** 22 June 2023.

extreme increases persist even when only looking at rainfall and not total precipitation, suggesting the presence of super-CC scaling effects. In contrast, on 28 June 2021, precipitation follows the expected CC scaling, increasing by $6.5\,\%\,\mathrm{K}^{-1}$. One possible explanation for the strong deviation on 22 June 2023 is the presence of a pronounced synoptic front. In line with 290 previous findings, such as those by Fowler et al. (2021), stronger synoptic-scale ascent and enhanced moisture convergence under warmer conditions may amplify convection and contribute to super-CC responses.

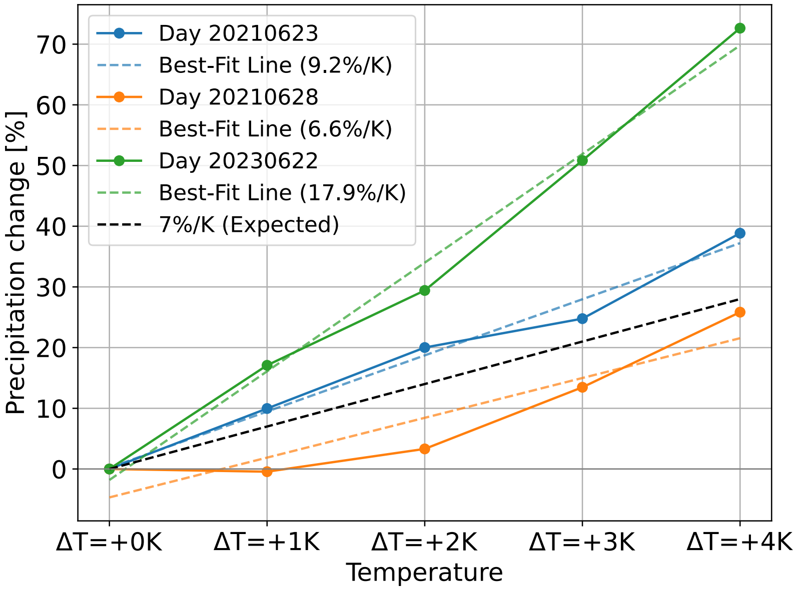

Figure 9. Percentage increase in total daily precipitation over the Germany domain and corresponding best-fit lines, compared to the expected Clausius–Clapeyron scaling of 7 % K^{-1}. Solid lines represent the percentage increase in precipitation over the entire day, while the dashed lines in matching colours show the respective best-fit trends. The domain is defined in Fig. 1.

This indicates that while CC scaling explains parts of the observed precipitation increase, additional dynamical and microphysical processes must be considered to account for the deviations beyond the thermodynamic expectation for Cases 1 and 3. Further investigation is required to identify the mechanisms driving these super-CC precipitation trends. The role of such processes is elaborated in the following sections.

It should be noted that the short predictability timescale of convective processes, particularly during initiation, can lead to non-linear responses. This inherent sensitivity may contribute to some of the amplified or variable trends observed in the simulations.

3.3 Convective Cell Frequency and Lifespan

To further analyse the occurrence of convective cells, version 1.5.3 of the Python package Tobac (Tracking and Object-Based Analysis of Clouds) (Heikenfeld et al., 2019; Sokolowsky et al., 2023) is used. Tobac is a software to identify, track, and analyse clouds and other meteorological phenomena such as updraughts, precipitation, and radiation. The tool uses algorithms to identify features and link them into consistent trajectories.

In this study, updraughts of cells at high temporal resolution (5 min) between 06:00 UTC and 24:00 UTC are tracked. For the updraught tracking, first, the data of the maximum updraught between 3 and 8 km height and the total condensate mixing ratio, which means the total amount of liquid and frozen water per mass of dry air, is calculated. Afterwards, several thresholds (3, 5,

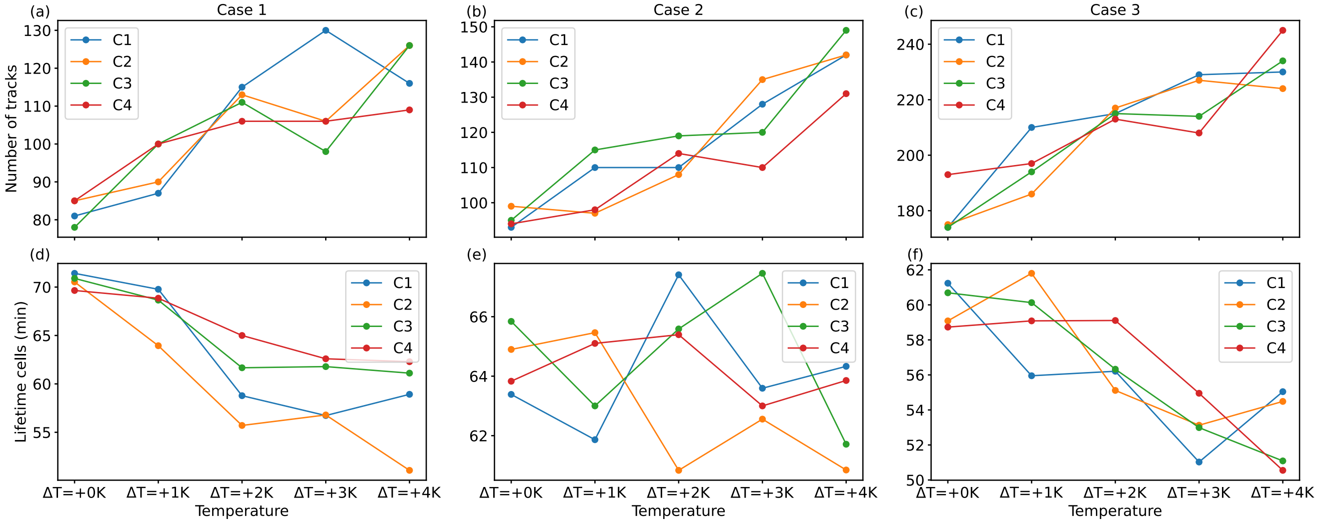

Figure 10. Number of tracks detected by the Tobac tool on (a) 23 June 2021, (b) 28 June 2021, and (c) 22 June 2023, and mean lifetimes of convective cells for all temperature regimes and CCN concentrations on (d) 23 June 2021, (e) 28 June 2021, and (f) 22 June 2023. All values are calculated between 06:00 UTC and 24:00 UTC. The MOSES domain was used for 23 and 28 June 2021, while the Germany domain was used for 22 June 2023. Line colours indicate the different CCN concentrations. The domain is defined in Fig. 1.

$10\,\mathrm{m\,s^{-1}}$) are used to track updraughts to better resolve overlapping cells. In addition, only updraughts with a minimum area of 10 grid cells are used as features, and a maximum distance of 25 grid cells is selected when linking features. As a segmentation threshold, a value of $0.5^{-3}\,\mathrm{kg\,kg^{-1}}$ is chosen as the condensate mixing ratio to identify the cloud volumes corresponding to the individual identified updraughts (Heikenfeld et al., 2019). To track only longer-lived cells, only tracks with a minimum lifetime of 30 min are used for the evaluation.

The simulated cells are further analysed by investigating how their number and lifetime are affected by temperature changes in the atmosphere (Fig. 10). All days show an increase in the number of convective cells and a decrease in their lifetime in simulations with higher temperatures. After investigating precipitation rates, an explanation for the shorter lifetimes of convective cells is found. Precipitation is found to start simultaneously across all investigated temperatures, with higher temperatures leading to greater peak intensities, followed by an earlier decline. This behaviour can be explained by the fact that higher temperatures enhance convective intensity, leading to a faster depletion of the available CAPE, even when overall CAPE is higher. This interpretation is supported by the observed increase in up- and downdraught velocities (Fig. 4), ultimately resulting in shorter cell lifetimes.

3.4 Aerosol-cloud interactions (ACI)

To gain an overview of how precipitation is affected by CCN concentration, changes in surface precipitation and total column-integrated parameters such as cloud water, rain, ice, snow, graupel, and hail are analysed (Fig. 11). Additionally, process rates

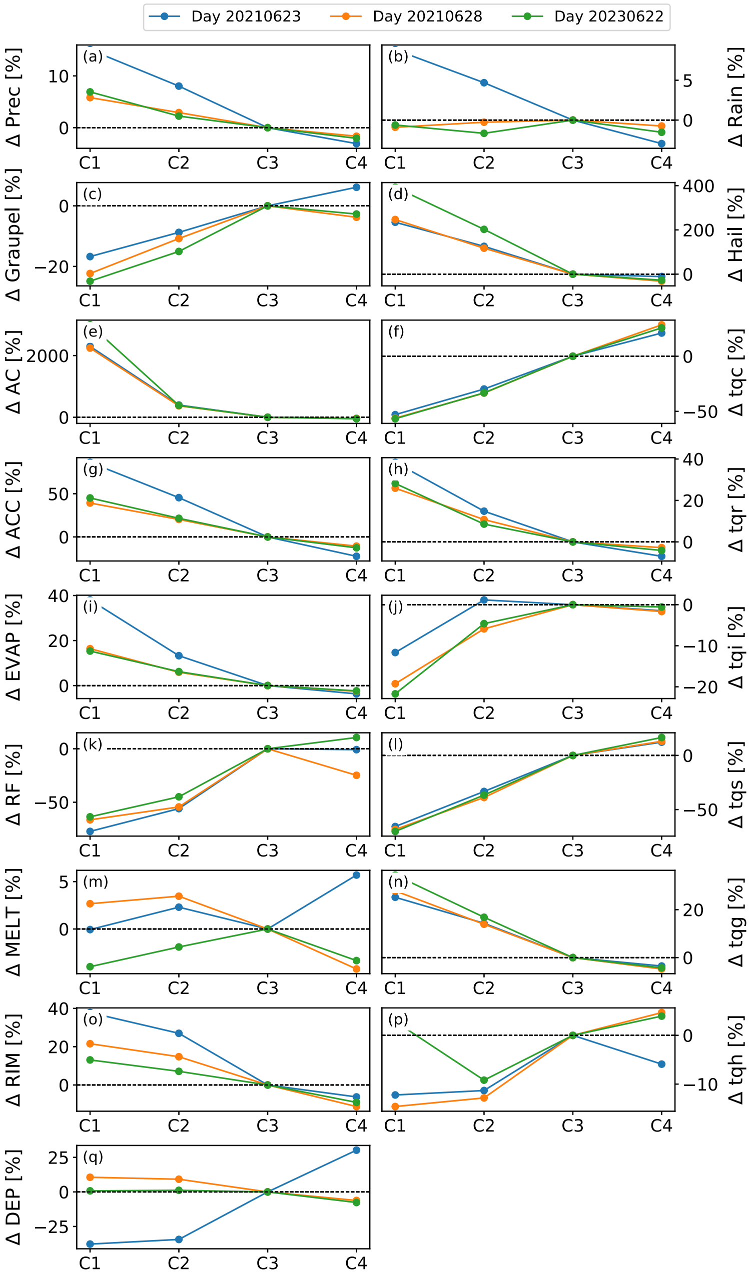

Figure 11. Percentage deviations of spatiotemporal averages of process rates such as autoconversion (AC), accretion (ACC), evaporation (EVAP), rain freezing (RF), melting (MELT), total riming (RIM), deposition (DEP) (left column) and of total column integrated cloud water (tqc), rain (tqr), ice (tqi), snow (tqs), graupel (tqg) and hail (tqh) amounts (right column) from the respective reference run with continental CCN concentration (C3).

of microphysical mechanisms are examined to explain the changes that have been observed. This analysis focuses on the results from the reference temperature simulations, as all temperature variations exhibited similar behaviour and, therefore, do not require a separate discussion. Following this analysis, the effects of temperature and CCN concentration on cold and warm rain formation processes, as well as on precipitation efficiency, are discussed.

3.4.1 Microphysical processes

Generally, a higher CCN concentration results in suppressed precipitation formation due to the more numerous but smaller cloud droplets, making the collision and coalescence process less efficient (Fan et al., 2017). Despite this initial suppression, the cold-phase convective invigoration theory suggests that delayed precipitation at high CCN levels can ultimately lead to more intense convection and stronger rainfall, along with the formation of more cold-phase hydrometeors (Rosenfeld et al., 2008). In contrast, lower CCN concentrations typically lead to fewer but larger cloud droplets, facilitating more efficient precipitation processes (Yau and Rogers, 1996).

In all three simulated cases, total precipitation decreases for higher CCN concentrations. Rain does not exhibit a clear trend, graupel increases, and hail shows a significant decrease of more than 200 % under higher CCN conditions (Fig. 11a-d). Higher CCN concentrations are expected to increase the number of cloud droplets while reducing their size, which may not always lead to a higher total cloud water mass. However, enhanced droplet nucleation can still result in increased column-integrated cloud water due to suppressed precipitation processes, a pattern that is observed across all three cases (Fig. 11f). Additionally, a decrease in the autoconversion and accretion processes is observed (Fig. 11e, g), both contributing to rain formation, explaining the decrease in rain within the atmosphere. At the same time, evaporation is enhanced for low CCN concentrations (Fig. 11i), which could explain why the increase in column-integrated rain for low CCN concentrations does not result in an increase in surface rain on all three days. Moreover, total column-integrated ice and snow (Fig. 11j, l) increases under polluted conditions, aligning with the cold-phase convection invigoration theory. This theory suggests that delayed precipitation formation allows cloud water to ascend to higher altitudes, transitioning into ice and other frozen hydrometeors. However, the cold-phase convection theory also predicts enhanced convection, which is not supported by the observed updraught intensities (not shown). Instead, a reversed trend emerges, with stronger up-and-downdraughts occurring at lower CCN concentrations.

These findings call into question the applicability of the cold-phase convective invigoration hypothesis in this context. While the theory proposes that increased aerosol concentrations enhance storm intensity through latent heat release during freezing, its overall validity remains uncertain. Numerous studies report contradictory results depending on cloud type, environmental conditions, and the choice of microphysical schemes (van den Heever et al., 2011; Altaratz et al., 2014; Fan et al., 2017). Recent theoretical work even suggests that aerosol-induced updraught enhancements may be significantly weaker or even negative than previously assumed (Altaratz et al., 2014; Igel and van den Heever, 2021). Rain freezing, deposition, and riming are all processes contributing to graupel and hail formation (Fig. 11k, q, o). The only hail production component that decreases significantly with higher CCN concentrations, mirroring the trend in surface hail content, is total riming, which exhibits an average change between 20 and 40 %. However, riming is the most significant contributor to hail and graupel formation, with a magnitude approximately four times greater than rain freezing and deposition. Consequently, rain freezing and deposition

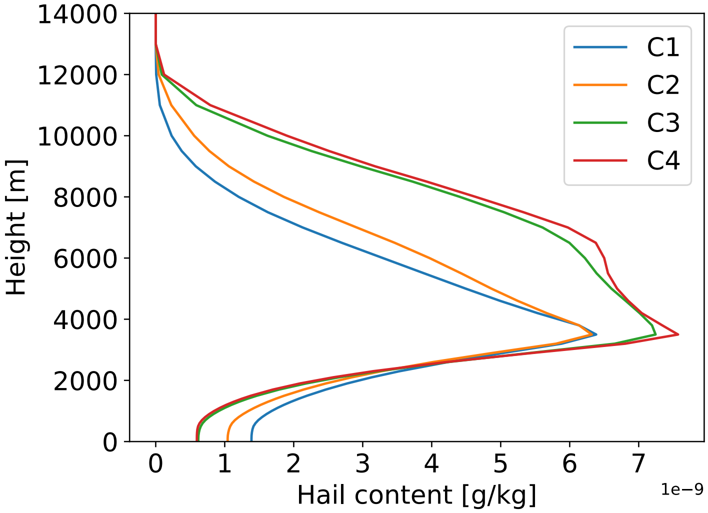

Figure 12. Vertical profiles of hail content for different CCN concentrations (23 June 2021).

have a negligible impact on hail formation. Interestingly, while column-integrated graupel content decreases in a high CCN environment within the column (Fig. 11n), hail content increases (Fig. 11p), which is the opposite of what occurs at the surface. Typically, a decrease in the total column would not be expected to correspond with an increase at the surface. To understand this behaviour, it is essential to consider the differences in hailstone sizes at varying CCN concentrations. This study previously found that hailstones grow larger in low CCN environments. Due to their lower surface-to-mass ratio, larger hailstones undergo less melting compared to smaller ones. This effect is evident in the vertical profile of atmospheric hail content (Fig. 12), which shows that in high CCN environments, where hailstones are smaller, increased melting occurs. Conversely, in low CCN environments, where hailstones are larger, melting is significantly reduced. As a result, larger hailstones are more likely to reach the surface under low CCN conditions.

Simultaneously, more graupel transforms into hail, while the remaining graupel melts before reaching the surface, leading to a decrease in surface graupel content under lower CCN conditions. This mechanism could also explain the overall relatively constant melting rates. However, since the output of the model does not differentiate between the melting rates of graupel and hail, direct verification of this hypothesis remains challenging.

3.4.2 Cold and warm rain

Rain can form through warm and cold processes. Given that the simulations are done for various temperatures and CCN concentrations, it is anticipated that the ratio between cold and warm rain formation will differ. This ratio is determined by dividing the contributions of processes that generate cold and warm rain, respectively, as follows:

$$\frac{\text{cold rain}}{\text{warm rain}} = \frac{\text{DEP}+\text{RIM}}{\text{AC}+\text{ACC}} \tag{6}$$

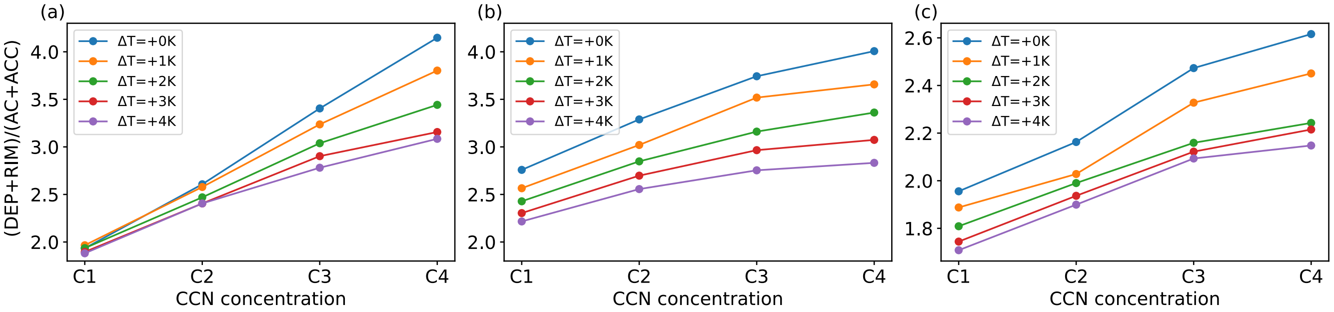

Figure 13. Cold-to-warm rain ratio (DEP+RIM)/(AC+ACC) for different CCN concentrations and temperatures on **(a)** 23 June 2021, **(b)** 28 June 2021, and **(c)** 22 June 2023.

DEP represents deposition, RIM denotes riming, and AC and ACC are autoconversion and accretion (Barthlott et al., 2022a). Figure 13 presents the results for each simulation day, showing variations in temperature and CCN concentrations. Across all days, higher CCN concentrations are associated with an increased cold-to-warm rain formation ratio, indicating a stronger contribution of cold rain processes. In contrast, higher temperatures lead to a reduction in this ratio. Note that the vertical axis for 22 June 2023 differs from the others, possibly due to the presence of strong synoptic forcing on that day.

Figure 14 displays the ratio of cold-to-warm rain formation processes, as a function of precipitation rate for the 23 June 2021 case. The ratio increases systematically with CCN concentration, from approximately 1.9 for C1 to over 4.1 for C4. This represents more than a twofold increase in the relative contribution of cold rain processes when moving from the lowest to the highest CCN scenario. This trend highlights the strong sensitivity of rain formation mechanisms to CCN concentrations: higher CCN concentrations suppress warm rain formation through delayed autoconversion and enhanced cloud droplet competition, thereby shifting precipitation generation toward cold processes such as deposition and riming. Importantly, the ratio remains remarkably stable across a broad range of precipitation rates above 0.2 mm per 30 min. This stability above a threshold suggests a robust shift in microphysical regimes primarily driven by CCN concentration, consistent with findings from Barthlott and Hoose (2018).

3.4.3 Precipitation efficiency

Another parameter important for precipitation formation is the precipitation efficiency, which is defined as the ratio of the precipitation P and the generation term G, including all processes that generate condensates in the atmosphere (Baur et al., 2022):

$$PE = \frac{P}{G} \tag{7}$$

The generation processes considered in this analysis include the microphysical processes of deposition, riming, autoconversion, and accretion. Fig. 15 shows the calculated precipitation efficiency (PE) on 23 June 2021 and the sensitivity to varying CCN concentrations, reflecting the relationship between condensate production and the amount of precipitation reaching the surface.

https://doi.org/10.5194/egusphere-2025-3069
Preprint. Discussion started: 10 July 2025

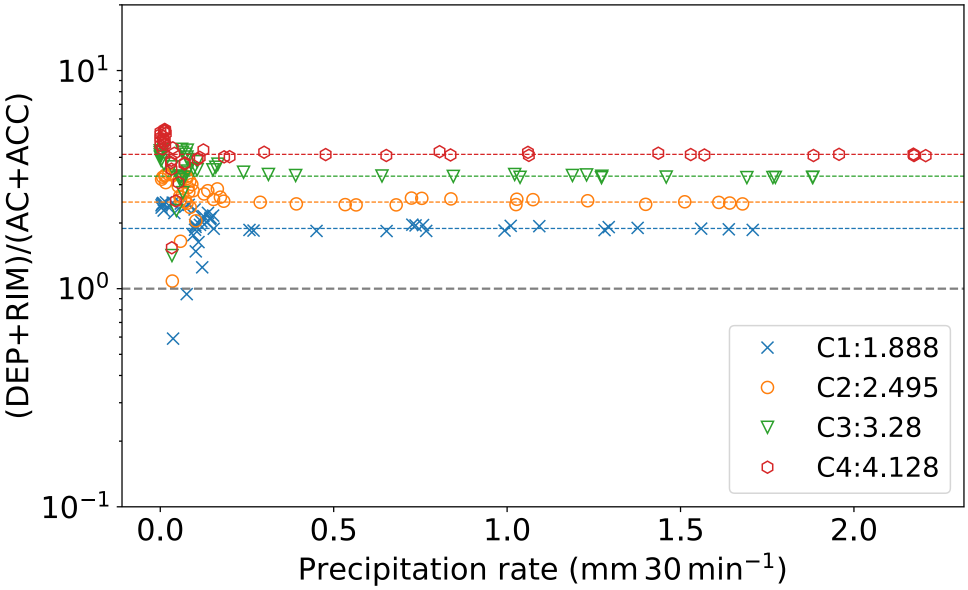

Figure 14. Cold-to-warm rain ratios (DEP+RIM)/(AC+ACC) plotted for each half an hour for different CCN concentrations (23 June 2021): C1 (blue cross), C2 (orange circle), C3 (green triangle), C4 (red hexagon). Dashed lines in the corresponding colour represent the mean taken for all data points having precipitation rates larger than 0.2 mm / 30 min. The legend shows the mean cold-to-warm rain ratios of each CCN concentration shown by the dashed lines.

An increase in PE is observed with higher CCN concentrations, indicating that a larger fraction of the formed hydrometeors reaches the surface. The generation term G (not shown) was also analysed separately and shows a decreasing trend with increasing CCN concentrations. Since total precipitation P depends on both PE and G, the net effect varies: if the increase in PE outweighs the decrease in G, precipitation increases and vice versa. In most simulations, precipitation decreases with higher CCN levels (not shown), except for Case 3, where precipitation remains nearly constant at +2 K and even increases at +3 K. Overall, the changes in precipitation remain relatively modest, typically within 10 %.

4 Summary and Conclusions

This study investigated how convective storms in Central Europe, especially supercells, would evolve under future climate conditions and environments with different aerosol loads. To explore these influences, this study conducted convection-resolving real-case simulations of supercell events previously observed during the Swabian MOSES field campaigns of 2021 and 2023. These events were simulated across five temperature scenarios, including a reference simulation, +1,+2,+3, and +4 K and four different CCN concentrations to observe storm behaviour under varied environmental conditions. The different CCN concentrations included values typically observed in Germany, providing a reliable reference point for comparison (Hande et al., 2015). The temperature perturbations were applied using the PGW approach, which isolates thermodynamic climate signals

https://doi.org/10.5194/egusphere-2025-3069
Preprint. Discussion started: 10 July 2025

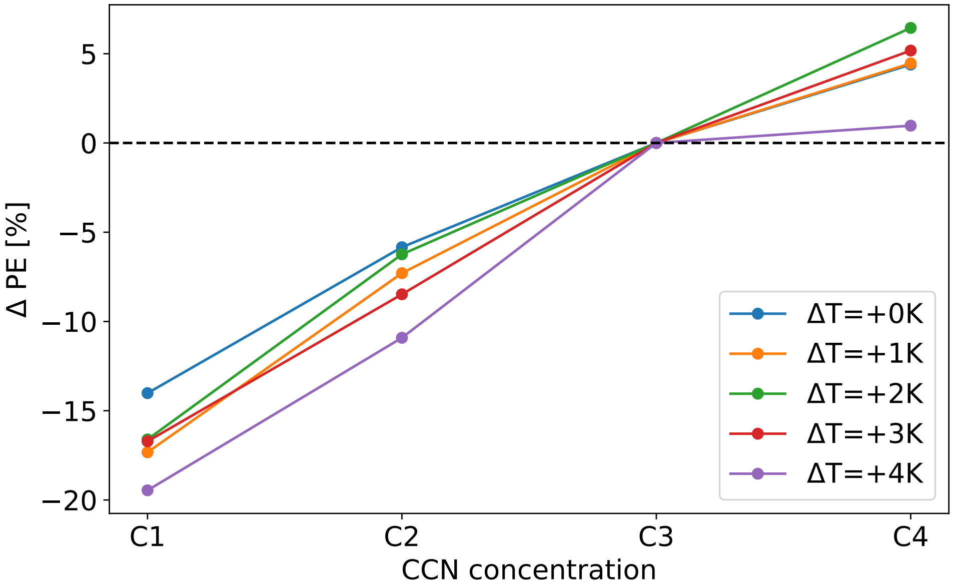

Figure 15. Precipitation efficiency of all four CCN concentrations for all simulation temperatures on 23 June 2021.

by consistently modifying initial and boundary conditions. This methodology enables a controlled investigation of the sensitivity of convective storm characteristics, such as storm intensity, duration, and convective precipitation, to future warming. By employing high-resolution, convection-resolving simulations on a 1 km grid, this research enables a detailed examination of convective processes, a depth of analysis that cannot be found in similar studies. This high-resolution model enables a comprehensive understanding of the dynamics of supercells and storm intensities in response to changing environmental conditions.

The results demonstrate that higher temperatures generally increase convective parameters such as CAPE and CIN, leading to more intense convection and a greater number of convective cells overall. This, in turn, accelerates the depletion of CAPE. The shorter lifetimes of convective cells in warmer environments further illustrate this effect. Other papers as Huang et al. (2024); Mallinson et al. (2024); Yang et al. (2024), also observed an increase in CAPE and CIN, suggesting a more favourable environment for stronger convective systems and less favourable ones for weaker systems.

Another important finding was the correlation of larger mean helicity values with increased atmospheric temperatures. Helicity values serve as indicators for updraught rotation and, therefore, supercells. Therefore, the simulations demonstrated that in a warmer environment, the likelihood of supercell development is increased, which leads either to more supercell formation, more intense supercells, or a combination of both. Furthermore, updraught intensity is increased in warmer environments, which supports the hypothesis of stronger convective cells.

The study also identified significant changes in precipitation amounts and the spatial distribution of rainfall in response to varying temperatures. As temperatures increased, total precipitation amounts generally rose, with both rain and hail exhibiting greater amounts. The analysis of the 95th percentile and the area that is affected by the 95th percentile both indicated a rise, which heightens the risk of flash floods. Additionally, for two of the three simulated cases, a super-CC scaling rate was observed, which means that the increase in precipitation can only be explained by additional factors beyond the increase in water vapour in the air column. Further analysis of hail characteristics indicates that higher temperatures and lower CCN concentrations, both anticipated in a future climate, lead to an increase in hailstone size, particularly for mean and large hailstones during convective events. This trend is especially concerning given the significant damage potential of larger hailstones.

The analysis of how ACI is influenced by varying CCN concentrations revealed several notable effects. Importantly, the influence of CCN on microphysical processes remains consistent across all temperature regimes. In high CCN environments, the processes of autoconversion and accretion, which are critical for warm rain formation, decrease, explaining the observed decrease in surface rainfall. The previously discussed decrease in hail was then explained by a reduced riming process, which is the dominant mechanism for hail formation. A closer examination of hail dynamics showed that there is more hail within the atmospheric column in environments with higher CCN concentrations. However, the amount of hail decreases at the surface compared to simulations with lower CCN concentrations. This counterintuitive result was explained by the smaller size of hailstones formed in high CCN conditions, which increases melting rates compared to the larger hailstones produced in low CCN environments.

These differences in formation processes result in an increased cold-to-warm rain formation ratio in environments with higher CCN concentrations and a decreased ratio in higher temperatures. Moreover, precipitation efficiency was considerably increased in environments with high CCN concentrations. As a result, while fewer hydrometeors were produced in high CCN concentration settings, a larger fraction of them reached the Earth's surface.

These findings indicate that convective storms, especially supercell events, will likely intensify, resulting in increased rainfall and larger hailstones. This intensification raises the risk of flash floods and poses a greater threat to property, agriculture, and infrastructure due to the heightened potential for severe weather impacts.

While this study provides valuable insights into the response of supercell storms to warming and aerosol changes, it is based on a limited set of three case studies. Additionally, the simulations assume constant relative humidity and apply only homogeneous warming, without considering vertical variations in temperature that would affect atmospheric stability. Large-scale dynamical changes are also not included. Despite these constraints, the results reveal clear and consistent trends, highlighting the robustness of the findings.

Code availability. This study is based on the ICON model version 2.6.6. The ICON model is available to the community under a permissive open source licence (BSD-3C) at https://gitlab.dkrz.de/icon/icon-model (DWD et al., 2024).

Data availability. The nature of the 4-D data generated in running the model experiments requires a large tape storage facility. These data are of the order of 200 TB (terabytes). The model data can be made available by the authors upon request. Global Forecast System (GFS) data is available through https://www.ncei.noaa.gov/products/weather-climate-models/global-forecast. The data needed to replicate the figures can be found at https://doi.org/10.5281/zenodo.15830656 (Lucas et al., 2025).

Author contributions. CB developed the project idea and designed the numerical experiments. LL performed the numerical simulations and conducted the analyses. LL wrote the paper with contributions from all co-authors.

Competing interests. The contact author has declared that none of the authors has any competing interests.

Acknowledgements. The authors thank the German Weather Service (DWD) for providing the ICON model code, the initial and boundary data, and the RADOLAN data. The field campaigns Swabian MOSES 2021 and 2023 were supported by funding from the Helmholtz Association within the framework of MOSES. The authors gratefully acknowledge the computing time made available to them on the high-performance computer HoreKa at the NHR Centre NHR@KIT. This centre is jointly supported by the Federal Ministry of Education and Research and the state governments participating in the NHR (www.nhr-verein.de/unsere-partner). This work was performed with the help of the Large Scale Data Facility at the Karlsruhe Institute of Technology, funded by the Ministry of Science, Research and the Arts Baden-Württemberg and by the Federal Ministry of Education and Research. The editing process was supported by OpenAI’s GPT-4, which was used to suggest revisions for language, structure, and readability. “Grammarly” generative AI (https://app.grammarly.com/) was used for the whole article’s grammar, spelling, and stylistic check.

References

Altaratz, O., Koren, I., Remer, L., and Hirsch, E.: Review: Cloud invigoration by aerosols—Coupling between microphysics and dynamics, Atmos. Res., 140-141, 38–60, https://doi.org/10.1016/j.atmosres.2014.01.009, 2014.

Ashley, W. S., Haberlie, A. M., and Gensini, V. A.: The future of supercells in the United States, Bulletin of the American Meteorological Society, 104, E1–E21, https://doi.org/https://doi.org/10.1175/BAMS-D-22-0027.1, 2023.

Barthlott, C. and Hoose, C.: Aerosol effects on clouds and precipitation over central Europe in different weather regimes, Journal of the Atmospheric Sciences, 75, 4247–4264, 2018.

Barthlott, C., Zarboo, A., Matsunobu, T., and Keil, C.: Impacts of combined microphysical and land-surface uncertainties on convective clouds and precipitation in different weather regimes, Atmospheric Chemistry and Physics, 22, 10 841–10 860, https://doi.org/https://doi.org/10.5194/acp-22-10841-2022, 2022a.

Barthlott, C., Zarboo, A., Matsunobu, T., and Keil, C.: Importance of aerosols and shape of the cloud droplet size distribution for convective clouds and precipitation, Atmospheric Chemistry and Physics, 22, 2153–2172, https://doi.org/https://doi.org/10.5194/acp-22-2153-2022, 2022b.

Barthlott, C., Czajka, B., Kunz, M., Saathoff, H., Zhang, H., Böhmländer, A., Gasch, P., Handwerker, J., Kohler, M., Wilhelm, J., et al.: The impact of aerosols and model grid spacing on a supercell storm from Swabian MOSES 2021, Quarterly Journal of the Royal Meteorological Society, 150, 2005–2027, https://doi.org/https://doi.org/10.1002/qj.4687, 2024.

Bauer, P., Thorpe, A., and Brunet, G.: The quiet revolution of numerical weather prediction, Nature, 525, 47–55, https://doi.org/10.1038/nature14956, 2015.

Baur, F., Keil, C., and Barthlott, C.: Combined effects of soil moisture and microphysical perturbations on convective clouds and precipitation for a locally forced case over Central Europe, Quarterly Journal of the Royal Meteorological Society, 148, 2132–2146, https://doi.org/https://doi.org/10.1002/qj.4295, 2022.

Brogli, R., Heim, C., Mensch, J., Sørland, S. L., and Schär, C.: The pseudo-global-warming (PGW) approach: methodology, software package PGW4ERA5 v1. 1, validation, and sensitivity analyses, Geoscientific Model Development, 16, 907–926, https://doi.org/https://doi.org/10.5194/gmd-16-907-2023, 2023.

Buizza, R.: Introduction to the special issue on "25 years of ensemble forecasting", Quarterly Journal of the Royal Meteorological Society, 145, 1–11, https://doi.org/https://doi.org/10.1002/qj.3370, 2019.

Chen, W., Cui, H., and Zheng, J.: Prediction of Clausius–Clapeyron scaling of daily precipitation extremes over China, Journal of Climate, 37, 165–177, 2024.

Chin, M., Diehl, T., Tan, Q., Prospero, J., Kahn, R., Remer, L., Yu, H., Sayer, A., Bian, H., Geogdzhayev, I., et al.: Multi-decadal aerosol variations from 1980 to 2009: a perspective from observations and a global model, Atmospheric Chemistry and Physics, 14, 3657–3690, 2014.

DWD, MPI, DKRZ, KIT, and C2SM: ICON Open Source Release, Gitlab [code], https://gitlab.dkrz.de/icon/icon-model, last access: 24 May 2024., 2024.

Fan, J., Wang, Y., Rosenfeld, D., and Liu, X.: Review of aerosol–cloud interactions: Mechanisms, significance, and challenges, Journal of the Atmospheric Sciences, 73, 4221–4252, https://doi.org/https://doi.org/10.1175/JAS-D-16-0037.1, 2016.

Fan, J., Leung, L. R., Rosenfeld, D., and DeMott, P. J.: Effects of cloud condensation nuclei and ice nucleating particles on precipitation processes and supercooled liquid in mixed-phase orographic clouds, Atmospheric Chemistry and Physics, 17, 1017–1035, https://doi.org/https://doi.org/10.5194/acp-17-1017-2017, 2017.

Fan, J., Zhang, Y., Wang, J., Jeong, J.-H., Chen, X., Zhang, S., Lin, Y., Feng, Z., and Adams-Selin, R.: Contrasting responses of hailstorms to anthropogenic climate change in different synoptic weather systems, Earth's Future, 10, e2022EF002 768, 2022.

Feng, Z., Chen, X., and Leung, L. R.: How Might the May 2015 Flood in the US Southern Great Plains Induced by Clustered MCSs Unfold in the Future?, Journal of Geophysical Research: Atmospheres, 129, e2023JD039 605, 2024.

Fowler, H. J., Lenderink, G., Prein, A. F., Westra, S., Allan, R. P., Ban, N., Barbero, R., Berg, P., Blenkinsop, S., Do, H. X., et al.: Anthropogenic intensification of short-duration rainfall extremes, Nature Reviews Earth & Environment, 2, 107–122, 2021.

Genz, C., Schrödner, R., Heinold, B., Henning, S., Baars, H., Spindler, G., and Tegen, I.: Estimation of cloud condensation nuclei number concentrations and comparison to in situ and lidar observations during the HOPE experiments, Atmospheric Chemistry and Physics, 20, 8787–8806, https://doi.org/https://doi.org/10.5194/acp-20-8787-2020, 2020.

Haerter, J. O. and Berg, P.: Unexpected rise in extreme precipitation caused by a shift in rain type?, Nature Geoscience, 2, 372–373, 2009.

Hande, L., Engler, C., Hoose, C., and Tegen, I.: Seasonal variability of Saharan desert dust and ice nucleating particles over Europe, Atmospheric Chemistry and Physics, 15, 4389–4397, https://doi.org/https://doi.org/10.5194/acp-15-4389-2015, 2015.

Handwerker, J., Barthlott, C., Bauckholt, M., Geppert, G., Hühn, E., Nallasamy, N. D., Dick, G., Dietrich, P., Güntner, A., Keller, J., Kunz, M., Landmark, S., Mohannazadeh, M., Morsy, M., Najafi, H., Oertel, A., Rakovec, O., Reich, H., Reich, M., Samaniego, L., Schrön, M., Schütze, C., Steinert, T., Vorogushyn, S., Weber, U., and Wieser, A.: From initiation of convective storms to their impact – The concept of the Swabian MOSES 2023 campaign, Front. Earth Sci., Submitted, 2024.

Hardwick Jones, R., Westra, S., and Sharma, A.: Observed relationships between extreme sub-daily precipitation, surface temperature, and relative humidity, Geophysical Research Letters, 37, 2010.

Heikenfeld, M., Marinescu, P. J., Christensen, M., Watson-Parris, D., Senf, F., van den Heever, S. C., and Stier, P.: tobac 1.2: towards a flexible framework for tracking and analysis of clouds in diverse datasets, Geoscientific Model Development, 12, 4551–4570, https://doi.org/https://doi.org/10.5194/gmd-12-4551-2019, 2019.

Heise, E., Ritter, B., Schrodin, R., and Wetterdienst, D.: Operational implementation of the multilayer soil model, Citeseer, 2006.

Hirt, M., Craig, G. C., Schäfer, S. A., Savre, J., and Heinze, R.: Cold-pool-driven convective initiation: Using causal graph analysis to determine what convection-permitting models are missing, Quarterly Journal of the Royal Meteorological Society, 146, 2205–2227, 2020.

Hoeppe, P.: Trends in weather related disasters–Consequences for insurers and society, Weather and climate extremes, 11, 70–79, https://doi.org/https://doi.org/10.1016/j.wace.2015.10.002, 2016.

Hogan, R. J. and Bozzo, A.: A Flexible and Efficient Radiation Scheme for the ECMWF Model, Journal of Advances in Modeling Earth Systems, 10, 1990–2008, https://doi.org/10.1029/2018MS001364, 2018.

Huang, Y., Xue, M., Hu, X.-M., Martin, E., Novoa, H. M., McPherson, R. A., Liu, C., Chen, M., Hong, Y., Perez, A., et al.: Increasing frequency and precipitation intensity of convective storms in the Peruvian Central Andes: Projections from convection-permitting regional climate simulations, Quarterly Journal of the Royal Meteorological Society, https://doi.org/https://doi.org/10.1002/qj.4820, 2024.

Igel, A. L. and van den Heever, S. C.: Invigoration or enervation of convective clouds by aerosols?, Geophysical Research Letters, 48, e2021GL093 804, 2021.

Kain, J. S., Weiss, S. J., Bright, D. R., Baldwin, M. E., Levit, J. J., Carbin, G. W., Schwartz, C. S., Weisman, M. L., Droegemeier, K. K., Weber, D. B., et al.: Some practical considerations regarding horizontal resolution in the first generation of operational convection-allowing NWP, Weather and Forecasting, 23, 931–952, 2008.

Kärcher, B. and Lohmann, U.: A parameterization of cirrus cloud formation: Homogeneous freezing of supercooled aerosols, Journal of Geophysical Research: Atmospheres, 107, AAC–4, https://doi.org/https://doi.org/10.1029/2001JD000470, 2002.

Kärcher, B., Hendricks, J., and Lohmann, U.: Physically based parameterization of cirrus cloud formation for use in global atmospheric models, Journal of Geophysical Research: Atmospheres, 111, https://doi.org/https://doi.org/10.1029/2005JD006219, 2006.

Khain, A., Beheng, K., Heymsfield, A., Korolev, A., Krichak, S., Levin, Z., Pinsky, M., Phillips, V., Prabhakaran, T., Teller, A., et al.: Representation of microphysical processes in cloud-resolving models: Spectral (bin) microphysics versus bulk parameterization, Reviews of Geophysics, 53, 247–322, https://doi.org/https://doi.org/10.1002/2014RG000468, 2015.

Kim, M. H., Lee, J., and Lee, S.-J.: Hail: Mechanisms, Monitoring, Forecasting, Damages, Financial Compensation Systems, and Prevention, Atmosphere, 14, 1642, https://doi.org/https://doi.org/10.3390/atmos14111642, 2023.

Kirshbaum, D. J., Adler, B., Kalthoff, N., Barthlott, C., and Serafin, S.: Moist orographic convection: Physical mechanisms and links to surface-exchange processes, Atmosphere, 9, 80, https://doi.org/https://doi.org/10.3390/atmos9030080, 2018.

Kröner, N., Kotlarski, S., Fischer, E., Lüthi, D., Zubler, E., and Schär, C.: Separating climate change signals into thermodynamic, lapse-rate and circulation effects: theory and application to the European summer climate, Climate Dynamics, 48, 3425–3440, https://doi.org/10.1007/s00382-016-3276-3, 2017.

Kunz, M. and Puskeiler, M.: High-resolution assessment of the hail hazard over complex terrain from radar and insurance data, Meteorologische Zeitschrift, 19, 427, https://doi.org/10.1127/0941-2948/2010/0452, 2010.

Kunz, M., Abbas, S. S., Bauckholt, M., Böhmländer, A., Feuerle, T., Gasch, P., Glaser, C., Groß, J., Hajnsek, I., Handwerker, J., et al.: Swabian MOSES 2021: An interdisciplinary field campaign for investigating convective storms and their event chains, Frontiers in Earth Science, 10, 999 593, https://doi.org/https://doi.org/10.3389/feart.2022.999593, 2022a.

Kunz, M., Abbas, S. S., Bauckholt, M., Böhmländer, A., Feuerle, T., Gasch, P., Glaser, C., Groß, J., Hajnsek, I., Handwerker, J., Hase, F., Khordakova, D., Knippertz, P., Kohler, M., Lange, D., Latt, M., Laube, J., Martin, L., Mauder, M., Möhler, O., Mohr, S., Reitter, R. W., Rettenmeier, A., Rolf, C., Saathoff, H., Schrön, M., Schütze, C., Spahr, S., Späth, F., Vogel, F., Völksch, I., Weber, U., Wieser, A., Wilhelm, J., Zhang, H., and Dietrich, P.: Swabian MOSES 2021: An interdisciplinary field campaign for investigating convective storms and their event chains, Front. Earth Sci., 10:999593, https://doi.org/10.3389/feart.2022.999593, 2022b.

Leibensperger, E. M., Mickley, L. J., Jacob, D. J., Chen, W.-T., Seinfeld, J., Nenes, A., Adams, P., Streets, D., Kumar, N., and Rind, D.: Climatic effects of 1950–2050 changes in US anthropogenic aerosols–Part 1: Aerosol trends and radiative forcing, Atmospheric Chemistry and Physics, 12, 3333–3348, https://doi.org/10.5194/acp-12-3333-2012, 2012.

Lenderink, G. and Van Meijgaard, E.: Increase in hourly precipitation extremes beyond expectations from temperature changes, Nature Geoscience, 1, 511–514, 2008.

Lenderink, G., Barbero, R., Loriaux, J., and Fowler, H.: Super-Clausius–Clapeyron scaling of extreme hourly convective precipitation and its relation to large-scale atmospheric conditions, Journal of Climate, 30, 6037–6052, 2017.

Leuenberger, D., Koller, M., Fuhrer, O., and Schär, C.: A generalization of the SLEVE vertical coordinate, Monthly Weather Review, 138, 3683–3689, https://doi.org/https://doi.org/10.1175/2010MWR3307.1, 2010.

Lin, Z., Nie, J., Wang, J., Chen, Y., and Meng, Z.: Responses of mesoscale convective system to global warming: A study on the Henan 2021 record-breaking rainfall event, Journal of Geophysical Research: Atmospheres, 129, e2023JD039 473, 2024.

Lucas, L., Barthlott, C., Hoose, C., and Knippertz, P.: Pseudo-Global Warming Simulations Reveal Enhanced Supercell Intensity and Hail Growth in a Future Central European Climate, https://doi.org/10.5281/zenodo.15830656, [data set], 2025.

Magnusson, L. and Källén, E.: Factors influencing skill improvements in the ECMWF forecasting system, Monthly Weather Review, 141, 3142–3153, https://doi.org/https://doi.org/10.1175/MWR-D-12-00318.1, 2013.

Mallinson, H., Lasher-Trapp, S., Trapp, J., Woods, M., and Orendorf, S.: Hailfall in a Possible Future Climate Using a Pseudo–Global Warming Approach: Hail Characteristics and Mesoscale Influences, Journal of Climate, 37, 527–549, https://doi.org/https://doi.org/10.1175/JCLI-D-23-0181.1, 2024.

Markowski, P. and Richardson, Y.: Mesoscale meteorology in midlatitudes, John Wiley & Sons, ISBN 978-0470742136, 2010.

Martinkova, M. and Kysely, J.: Overview of observed Clausius-Clapeyron scaling of extreme precipitation in midlatitudes, Atmosphere, 11, 786, 2020.

Púčik, T., Castellano, C., Groenemeijer, P., Kühne, T., Rädler, A. T., Antonescu, B., and Faust, E.: Large hail incidence and its economic and societal impacts across Europe, Monthly Weather Review, 147, 3901–3916, https://doi.org/https://doi.org/10.1175/MWR-D-19-0204.1, 2019.

Puskeiler, M., Kunz, M., and Schmidberger, M.: Hail statistics for Germany derived from single-polarization radar data, Atmospheric Research, 178, 459–470, https://doi.org/https://doi.org/10.1016/j.atmosres.2016.04.014, 2016.

Rädler, A. T., Groenemeijer, P., Faust, E., and Sausen, R.: Detecting severe weather trends using an additive regressive convective hazard model (AR-CHaMo), Journal of Applied Meteorology and Climatology, 57, 569–587, https://doi.org/https://doi.org/10.1175/JAMC-D-17-0132.1, 2018.

Raschendorfer, M.: The new turbulence parameterization of LM, https://www.cosmo-model.org, 2001.

Rasmussen, K. L., Prein, A. F., Rasmussen, R. M., Ikeda, K., and Liu, C.: Changes in the convective population and thermodynamic environments in convection-permitting regional climate simulations over the United States, Climate Dynamics, 55, 383–408, https://doi.org/10.1007/s00382-017-4000-7, 2020.

Raupach, T. H., Martius, O., Allen, J. T., Kunz, M., Lasher-Trapp, S., Mohr, S., Rasmussen, K. L., Trapp, R. J., and Zhang, Q.: The effects of climate change on hailstorms, Nature reviews earth & environment, 2, 213–226, https://doi.org/https://doi.org/10.1038/s43017-020-00133-9, 2021.

Risser, M. D. and Wehner, M. F.: Attributable human-induced changes in the likelihood and magnitude of the observed extreme precipitation during Hurricane Harvey, Geophysical Research Letters, 44, 12–457, 2017.

Rosenfeld, D., Lohmann, U., Raga, G. B., O'Dowd, C. D., Kulmala, M., Fuzzi, S., Reissell, A., and Andreae, M. O.: Flood or drought: how do aerosols affect precipitation?, science, 321, 1309–1313, https://doi.org/10.1126/science.1160606, 2008.

Schär, C., Frei, C., Lüthi, D., and Davies, H. C.: Surrogate climate-change scenarios for regional climate models, Geophysical Research Letters, 23, 669–672, https://doi.org/https://doi.org/10.1029/96GL00265, 1996.

Schmid, T., Portmann, R., Villiger, L., Schröer, K., and Bresch, D. N.: An open-source radar-based hail damage model for buildings and cars, Natural Hazards and Earth System Sciences, 24, 847–872, https://doi.org/https://doi.org/10.5194/nhess-24-847-2024, 2024.

Segal, Y. and Khain, A.: Dependence of droplet concentration on aerosol conditions in different cloud types: Application to droplet concentration parameterization of aerosol conditions, Journal of Geophysical Research: Atmospheres, 111, 2006.

Seifert, A. and Beheng, K. D.: A two-moment cloud microphysics parameterization for mixed-phase clouds. Part 1: Model description, Meteorology and atmospheric physics, 92, 45–66, https://doi.org/10.1007/s00703-005-0112-4, 2006.

Seifert, A., Köhler, C., and Beheng, K.: Aerosol-cloud-precipitation effects over Germany as simulated by a convective-scale numerical weather prediction model, Atmospheric Chemistry and Physics, 12, 709–725, https://doi.org/https://doi.org/10.5194/acp-12-709-2012, 2012.

Semie, A. G. and Bony, S.: Relationship between precipitation extremes and convective organization inferred from satellite observations, Geophysical Research Letters, 47, e2019GL086 927, 2020.

Smith, S. J., van Aardenne, J., Klimont, Z., Andres, R. J., Volke, A., and Delgado Arias, S.: Anthropogenic sulfur dioxide emissions: 1850–2005, Atmospheric Chemistry and Physics, 11, 1101–1116, https://doi.org/10.5194/acp-11-1101-2011, 2011.

Sokolowsky, G. A., Freeman, S. W., Jones, W. K., Kukulies, J., Senf, F., Marinescu, P. J., Heikenfeld, M., Brunner, K. N., Bruning, E. C., Collis, S. M., et al.: tobac v1. 5: Introducing Fast 3D Tracking, Splits and Mergers, and Other Enhancements for Identifying and Analysing Meteorological Phenomena, EGUsphere, 2023, 1–37, https://doi.org/https://doi.org/10.5194/egusphere-2023-1722, 2023.

Tahara, R., Hiraga, Y., and Kazama, S.: Climate change effects on the localized heavy rainfall event in northern Japan in 2022: Uncertainties in a pseudo-global warming approach, Atmospheric Research, 314, 107 780, 2025.

Tao, W.-K., Li, X., Khain, A., Matsui, T., Lang, S., and Simpson, J.: Role of atmospheric aerosol concentration on deep convective precipitation: Cloud-resolving model simulations, Journal of Geophysical Research: Atmospheres, 112, https://doi.org/https://doi.org/10.1029/2007JD008728, 2007.

Taszarek, M., Allen, J., Púčik, T., Groenemeijer, P., Czernecki, B., Kolendowicz, L., Lagouvardos, K., Kotroni, V., and Schulz, W.: A climatology of thunderstorms across Europe from a synthesis of multiple data sources, Journal of Climate, 32, 1813–1837, https://doi.org/https://doi.org/10.1175/JCLI-D-18-0372.1, 2019.

Thomas, J., Barrett, A., and Hoose, C.: Temperature and cloud condensation nuclei (CCN) sensitivity of orographic precipitation enhanced by a mixed-phase seeder–feeder mechanism: a case study for the 2015 Cumbria flood, Atmospheric Chemistry and Physics, 23, 1987–2002, https://doi.org/https://doi.org/10.5194/acp-23-1987-2023, 2023.

Thompson, R. L., Mead, C. M., and Edwards, R.: Effective storm-relative helicity and bulk shear in supercell thunderstorm environments, Weather and forecasting, 22, 102–115, https://doi.org/https://doi.org/10.1175/WAF969.1, 2007.

Trapp, R. J., Hoogewind, K. A., and Lasher-Trapp, S.: Future changes in hail occurrence in the United States determined through convection-permitting dynamical downscaling, Journal of Climate, 32, 5493–5509, https://doi.org/https://doi.org/10.1175/JCLI-D-18-0740.1, 2019.

van den Heever, S. C., Stephens, G. L., and Wood, N. B.: Aerosol indirect effects on tropical convection characteristics under conditions of radiative-convective equilibrium, Journal of the Atmospheric Sciences, 68, 699–718, 2011.

Van Oldenborgh, G. J., Krikken, F., Lewis, S., Leach, N. J., Lehner, F., Saunders, K. R., Van Weele, M., Haustein, K., Li, S., Wallom, D., et al.: Attribution of the Australian bushfire risk to anthropogenic climate change, Natural Hazards and Earth System Sciences Discussions, 2020, 1–46, 2020.

Watson-Parris, D. and Smith, C. J.: Large uncertainty in future warming due to aerosol forcing, Nature Climate Change, 12, 1111–1113, 2022.

Weisman, M. L. and Rotunno, R.: The use of vertical wind shear versus helicity in interpreting supercell dynamics, Journal of the atmospheric sciences, 57, 1452–1472, https://doi.org/https://doi.org/10.1175/1520-0469(2000)057<1452:TUOVWS>2.0.CO;2, 2000.

Yang, Z., Wang, J., Qian, Y., Chakraborty, T., Xue, P., Pringle, W. J., Huang, C., Kayastha, M. B., Huang, H., Li, J., et al.: Summer convective precipitation changes over the Great Lakes region under a warming scenario, Journal of Geophysical Research: Atmospheres, 129, e2024JD041 011, https://doi.org/https://doi.org/10.1029/2024JD041011, 2024.

Yau, M. K. and Rogers, R. R.: A short course in cloud physics, Elsevier, 1996.

Yli-Juuti, T., Mielonen, T., Heikkinen, L., Arola, A., Ehn, M., Isokääntä, S., Keskinen, H.-M., Kulmala, M., Laakso, A., Lipponen, A., et al.: Significance of the organic aerosol driven climate feedback in the boreal area, Nature Communications, 12, 5637, 2021.

Zängl, G., Reinert, D., Rípodas, P., and Baldauf, M.: The ICON (ICOsahedral Non-hydrostatic) modelling framework of DWD and MPI-M: Description of the non-hydrostatic dynamical core, Quarterly Journal of the Royal Meteorological Society, 141, 563–579, https://doi.org/https://doi.org/10.1002/qj.2378, 2015.